Nanostructured Pd barrier for low methanol crossover DMFC

A. Casalegno [a,*], F. Bresciani [a], V. Di Noto [b,c], C.S. Casari [a], A. Li Bassi [a], E. Negro [b,c], R. Marchesi [a], F. Di Fonzo [d]

[a] Politecnico di Milano, Department of Energy, 20156 Milano, Italy
[b] Department of Chemical Sciences, University of Padova, Italy
[c] Consorzio Interuniversitario Nazionale per la Scienza e la Tecnologia dei Materiali, INSTM, Italy
[d] Center for Nano Science and Technology – ITT@PoliMi, Istituto Italiano di Tecnologia, Italy

Received 12 April 2013
Received in revised form
27 July 2013
Accepted 6 September 2013
Available online 5 October 2013

1. Introduction

Direct methanol fuel cells (DMFCs) are a promising technology for portable and small stationary applications, due to the advantages of a liquid and readily-available fuel [1]. At the moment DMFCs are studied in a wide and growing number of research projects for portable and small stationary power supply, a short-term application, where cost and technical requirements are close to be achieved. To be competitive in portable applications and in general to improve DMFC performance, some technical challenges that strongly reduce efficiency and power density have to be overcome, with a particular reference to the low rate of methanol oxidation kinetics on the anode and the methanol crossover through the polymeric membrane [2]. Methanol crossover occurs due to the inability of the commonly used proton-conducting polymeric membranes to prevent methanol from permeating their structure; diffusion and electro-osmotic drag are the primary driving forces for methanol transport through the proton-conducting polymeric membrane [3,4]. Methanol reacts with platinum catalyst sites on the cathode, leading to a mixed potential on the cathode and a lower oxygen availability for the electro–chemical reaction [5,6].

Methanol crossover in DMFCs has been recently studied both experimentally and theoretically [2–6]; different reports confirm that methanol diffusion is generally the dominant contribution. Research activities to reduce crossover are focussing on membrane formulation and other types of

* Corresponding author. Tel.: +39 (0)223993912; fax: +39 (0)223993913.
E-mail addresses: andrea.casalegno@polimi.it, casalegno.andrea@gmail.com (A. Casalegno).

methanol permeation barriers. A number of techniques has been reported recently. One of them is to modify proton-conducting electrolyte membranes based on Nafion™. Antonucci et al. [7] prepared a Nafion-silica composite electrolyte membrane and a Nafion-zirconium phosphate composite membrane [8], both of which had lower methanol permeation than Nafion. DMFCs including these membranes could be operated at a high temperature of 140–150 °C. Uchida et al. [9] dispersed Pt nanocrystal particles in Nafion117™ to suppress methanol permeation. Jia et al. [10] modified Nafion117™ by impregnating the membrane with poly(1-methylpyrrole) by "*in-situ*" polymerization. Although the methanol crossover was decreased in their modified membrane, its conductivity became lower. On the other hand, Peled et al. [11] developed a novel low-cost nanoporous proton-conducting membrane consisting of high-surface-area inorganic powders such as silica, and polymer binders like polyvinylidene fluoride (PVDF).

In general, the experimental results showed that this kind of membranes are characterized by a lower methanol crossover but also by an important reduction in proton conductivity. An alternative approach consists in modifying the features of the anodic transport layer; however, reduction is still limited to less than 50% [12]. Another recent and innovative approach is to produce barriers to prevent methanol crossover by means of a methanol-impermeable proton conducting (MIPC) layer. Thin films of Pd and Pd alloys look as promising candidates in this respect since hydrogen in palladium behaves like a proton [13], so this kind of metal or alloy membranes may be considered as a proton exchange membrane. Although the cell with the Pd-sputtered membrane exhibited superior performance, the repeated hydride formation in the Pd thin layer during the continuous operation of the cell may lead to hydrogen embrittlement in the Pd thin layer, due to $\alpha \rightarrow \beta$ phase transition at low temperatures (<150 °C). This, in turn, can cause the mechanical delamination of the Pd layers from the surface of the membrane. This problem is known in other fields of application and several solutions have been proposed, mainly alloying Pd with Ag (30 wt%), Cu (40 wt%) and Au (5 wt%). Alloys of Pd–Ag [14] and Pd–Cu [15] sputtered on standard Nafion have been tested. Pd–Ag shows a higher proton conductivity than Pd–Cu [16].

Even though they are very promising, these works failed to obtain a complete blockage of methanol crossover. This is mainly attributed to the high density of wide cracks (200–300 nm) present on the reported films. It is believed that the cracks were caused by the residual stress between the sputtering layer and the Nafion polymer membrane during the sputtering process. Since sputtering is generally carried out under medium vacuum conditions (1–10^{-3} mbar), the polymer substrate might become completely dry without moisture, thus shrinking. When samples are exposed to ambient air they re-absorb water moisture, leading to expansion. In the meantime, the sputtered metal layer is insensitive to the environmental condition; thus, its volume would remain more or less the same after the sputtering process. Therefore, a mismatch might be caused between the expanded polymer substrate and the metal barrier, leading to the thin layer cracking. The other fundamental issue in using the sputtering technique is its limited capacity of depositing films with a controlled porosity and nanostructure, thus limiting the possible strategies to solve the problem.

This work aims to demonstrate that the Pulsed Laser Deposition technique (PLD) is able to solve these issues and to produce Pd barriers with controlled characteristics on a standard membrane even at pressures of several Pascal. The preliminary results of materials characterization and fuel cell testing are reported and discussed.

2. Experimental

2.1. *Preparation of the samples*

Nafion117™ membranes were procured from Quintech. Each Nafion117™ membrane was successively boiled for 30′ in 5% H_2O_2, deionized (DI) water, 1 M H_2SO_4, and DI water. After this wet conditioning, the membrane was dried in air overnight. Upon mounting on the 2″ PLD substrate holder, a wet tissue was placed in between the conditioned membrane and the holder in order to keep hydrated the membrane during the PLD deposition. Palladium barrier films were deposited at room temperature on the membrane by ablating a Pd target with a ns-pulsed laser (Nd:YAG by Continuum, $\lambda = 266$ nm, $f_p = 10$ Hz, pulse duration ≈ 6 ns) in vacuum. The fluence on the target was 2 $J \cdot cm^{-2}$ and the background gas (He, purity 99,9999%) pressure was varied from 1 Pa to 400 Pa. Deposition distance was varied between 3 and 7 cm, but optimal results, shown here, were achieved at 3 cm. The number of laser pulses was varied in order to obtain the desired film thickness. Off-axis deposition and substrate rotation were implemented in order to obtain an uniform deposition on the 2″ active area. More specifically, the off axis position was adjusted in order to have a radial thickness uniformity in the order of 10–20%, depending on the other deposition parameters, most significantly the background gas pressure.

2.2. *Instruments and methods*

Scanning Electron Microscopy (SEM) images were acquired on deposited barriers and some tested samples by a Zeiss SUPRA 40 Field-Emission SEM equipped with a pole piece mounted solid-state Back Scattered Electrons (BSE) detector. Structural characterization was performed via XRD analysis, which was carried out using a PANalytical X'Pert PRO x-ray diffractometer in $\theta/2\theta$ configuration, with a solid state X'Celerator detector. Spectra were collected using Cu K_α (1.54 A°) radiation. Atomic Force Microscope images were acquired with a Thermomicroscope Autoprobe CP Research in non-contact mode.

The collection of dynamic mechanical analysis (DMA) data was executed by means of a TA Instruments DMA Q800 instrument using the film/fiber tension clamp. The temperature spectra were determined by subjecting a rectangular dry film sample of ca. 25 (height) mm × 6 (width) mm × 0.2 (thickness) mm to an oscillatory sinusoidal tensile deformation with an amplitude of 4 mm at 1 Hz and with a 0.05 N preload force. The temperature range spanned from −10–180 °C, and was

covered at a rate of 4 °C·min^{-1}. The elastic (storage) (E′) and viscous (loss) modulus (E″) were at the basis of the analysis of the mechanical response of the materials. tan δ = E″/E′ was analyzed as a function of the temperature to evaluate the material damping features.

The measurements of complex conductivity spectra by Broadband Electrical Spectroscopy (BES) were executed with an Agilent 4294A analyzer in the frequency range between 40 Hz and 10 MHz. A home-made cryostat operating with a N_2 gas jet heating and cooling system was adopted to explore a temperature range from 5 to 155 °C. The measurements were carried out with a sealed home-made cell, both on pristine and on hydrated membranes. The hydrated membranes were obtained by autoclaving the pristine membranes at RH 100%, T = 135 °C and P = 3.3 bar. The hydrated membranes were maintained wet during the measurements as follows. The hydrated membrane was sandwiched between two circular platinum electrodes and placed inside a cylindrical Teflon cell. This setup was adopted to study the through-plane electric properties of the membranes, as an effective approximation of the operating fuel cell. The free volume of the cell was partially filled with 100 μL of bidistilled water to prevent drying in measurements carried out at temperatures as high as 155 °C. The geometrical constant of the cell was determined by measuring the electrode–electrolyte contact surface and the distance between electrodes with a micrometer. The temperature measurement was executed with an accuracy greater than ±0.05 °C. No water was lost during the measurements, as checked by weighing the closed cell before and after the measurements. The complex impedance ($Z(\omega)$) was converted into complex conductivity ($\sigma^*(\omega) = \sigma'(\omega) + i\sigma''(\omega)$) using the equation $\sigma^*(\omega) = k \cdot [Z^*(\omega)]^{-1}$; ($Z^*(\omega) = Z'(\omega) + iZ''(\omega)$), where k is the cell constant in cm^{-1} and $\omega = 2\pi f$ (f = frequency in Hz). The bulk through-plane conductivity of the materials, σ_{DC}, was determined by measuring the conductivity value interpolated in the plateau of the $\sigma'(\omega)$ profiles at frequencies higher than 10^5 Hz, as described elsewhere [17,18].

2.3. Fabrication of membrane electrode assemblies and characterization in single fuel cell

The experimental analyses of DMFC performance and methanol crossover are carried out utilizing the same equipment and methodologies presented in a previous study [12]. Membrane proton resistance is estimated measuring fuel cell internal resistance at 1 kHz with an AC milliohmeter during fuel cell operation. The MEAs present an active area of 4 cm^2 and are tested in the operating conditions reported in Table 1.

The membrane prepared as previously described are coated with a further Nafion112™ membrane over the Pd film to ensure the suitable electrolyte contact with the electrodes. The MEAs are assembled utilizing commercial gas diffusion electrodes: anode catalysed layer presents a metal loading of 2 mg cm^{-2} (Pt:Ru = 2) coated on SGL10AC (300 μm, 10% PTFE) backing layer, cathode catalysed layer presents a metal loading of 1.3 mg cm^{-2} (Pt) coated on SGL10CC (300 μm, 10% PTFE with microporous layer) backing layer. Cell gaskets consist in a Mylar layer (thickness 50 μm), in contact with the membrane, and a fibreglass layer covered by PTFE (thickness 250 μm).

Table 1 – Fuel Cell operating conditions.

Controlled parameter	Investigated range	Uncertainty
Voltage, V	0.1–0.6 V	0.5% + 1 mV
Fuel cell temperature, T	333–353 K	0.1 K
Methanol mass fraction, X	3.25–6.5%w	0.07%w
Anode flow rate, m_{met}	0.5 g/min	1.5%
Anode mean pressure, P_a	101 kPa	5 kPa
Air flow rate, m_{air}	0.206 g/min	1% + 0.005 g/min
Cathode mean pressure[a], P_c	105	5 kPa

[a] Cathode mean pressure is calculated as the mean value between inlet and outlet pressures.

3. Results and discussion

3.1. Characterization of the Pd barriers

In Pulsed Laser Deposition (PLD), an excimer laser ablates a target of the material that is to be deposited inside a vacuum chamber which can be filled with the desired gas. The laser locally ablates the target and creates a plasma that expands supersonically due to a density gradient between the solid surface of the target and the environment in which the whole process is performed. The ablated species condense onto the substrate sample, where a thin film is formed. By varying the background gas pressure and the laser power it is possible to induce cluster nucleation in the expanding plume and to fine-tune the kinetic energy and the deposition mechanisms of the nanoparticles, thus achieving a good control of the morphology of the deposit.

As in any other vapour phase deposition technique, in PLD film morphology and grain size are controlled by the kinetic energy of impinging atoms and by the temperature of the substrate surface. When the latter temperature is kept low (typically below a fifth of the melting temperature of the material to be deposited), a reduced surface diffusion of the incoming species leads to pinning and, subsequently, to the growth of columnar or even porous microstructures. This well-established film evolution was described in a structure zone diagram (SZD) by Movchan and Demchishin Ref. [19] for evaporated films and by Thornton [20] for sputtered films. Recently, Infortuna et al. [21] described the microstructure evolution of CGO (Cerium Gadolinium Oxide) and YSZ (Yttria Stabilized Zirconia) ceramic films deposited by PLD in function of substrate temperature.

Nevertheless, PLD is characterized by a supersaturated pulsed flux and hyperthermal species [22] that can give rise to dense, nanocrystalline ceramic films even at room temperature [23]. By tuning PLD deposition conditions, namely pressure, target to substrate distance and laser fluence, it is possible [24,25] to fine-tune film microstructure and mechanical properties of metal oxides. In this study, we show for the first time that, for a given set of deposition parameters, a

similar control is achievable on the micro- and nanostructure of metallic thin films by varying the He pressure in the deposition chamber during deposition. Nafion117™ and Si were used as substrates. It is found that a threshold pressure, around 100 Pa, exists below which deposited films are dense and nanocrystalline (Fig. 1 a) to c); film deposited at 10^{-3} Pa) and above which are porous, columnar and ultrafine grained (Fig. 1 d) to *f*) film deposited at 100 Pa). In Fig. 2a) the evolution of the diffractogram with pressure is presented for 100 nm thick films. Only the diffraction peak at $2\theta = 40.11°$, corresponding to the (111) plane of the cubic Pd lattice, is clearly detectable in all the spectra. The (200) diffraction peak at $2\theta = 46.66°$ is barely visible only in the most crystalline samples. Calculating the grain size with the Scherrer formula, a diminishing of crystalline domain size with pressure is observed (Fig. 2b)). The latter occurrence and the onset of the columnar and porous morphology are a consequence of the reduced kinetic energy of the Pd species (atoms and clusters) impinging on the substrate with increasing pressure, due to the energy loss and scattering upon interaction with the background gas in the deposition chamber.

Direct imaging of the nanograins was achieved in the SEM in channelling contrast mode at 0° tilt [26]. The size found for the low c) and high *f*) pressure deposited films matches the one obtained by the analysis of the XRD data. In this imaging mode the intergrain nanoporosity (Fig. 1f)) is evident. A thickness dependence study of grain size has been undertaken for a fixed He pressure value of 50 Pa (Fig. 2c)). An increase in grain size with thickness is found. Interestingly, films grown on Si and Nafion117™ membranes exhibit the same trend with a tendency to saturation for the thicker films. This could be attributed to the high pinning rate induced by the nature and low temperature of the substrate. With increasing thickness the effect of the low temperature of the substrate vanishes and the diffusivity of the impinging Pd species on the growing Pd surface increases, leading to a larger grain size.

Fundamental for this work has been the proper treatment of the Nafion117™ membranes prior to and during deposition, in order to minimize residual stresses, clean the surface and bring the substrate to a dimension close to the in cell operation.

Pd films grown directly on the Nafion117™ membranes exhibit a smooth and continuous appearance with no sign of cracks even after storage in ambient conditions for several days. This case is shown in Fig. 3a). The lines visible in the optical micrograph are wrinkles of the metallic film, as shown in the AFM image and line scan in Fig. 3b and c). The origin of these wrinkles are attributed to the buckling of the metallic film under compressive stress exerted by the Nafion117™ membrane dehydrating during the storage. In Fig. 3b), as already stated, the Pd film on Nafion grows in a similar manner as on Si subsrate. The XRD of a 120 nm film deposited at 50 Pa on Nafion membrane is shown in Fig. 2d).

3.2. *Characterization of the membranes*

The trends of the storage modulus E′, of the loss modulus E″ and of tan δ as a function of the temperature are plotted in Fig. 4. The maximum of tan δ is known as the α_{PC} relaxation peak [27]; it is attributed to the long-range motions of both the fluorocarbon backbone and the perfluoroethereal side chains of Nafion. These long-range motions are facilitated when the electrostatic interactions occurring within the polar domains of Nafion are weakened [3]. On these bases, it can be assumed that the treatments adopted to prepare all the barriers give rise to the formation of additional crosslinks within the polar domains of Nafion; as a result, the overall strength of the electrostatic interactions is increased [27]. Thus, in all the barriers the temperature of the α_{PC} relaxation peak (~105 °C)

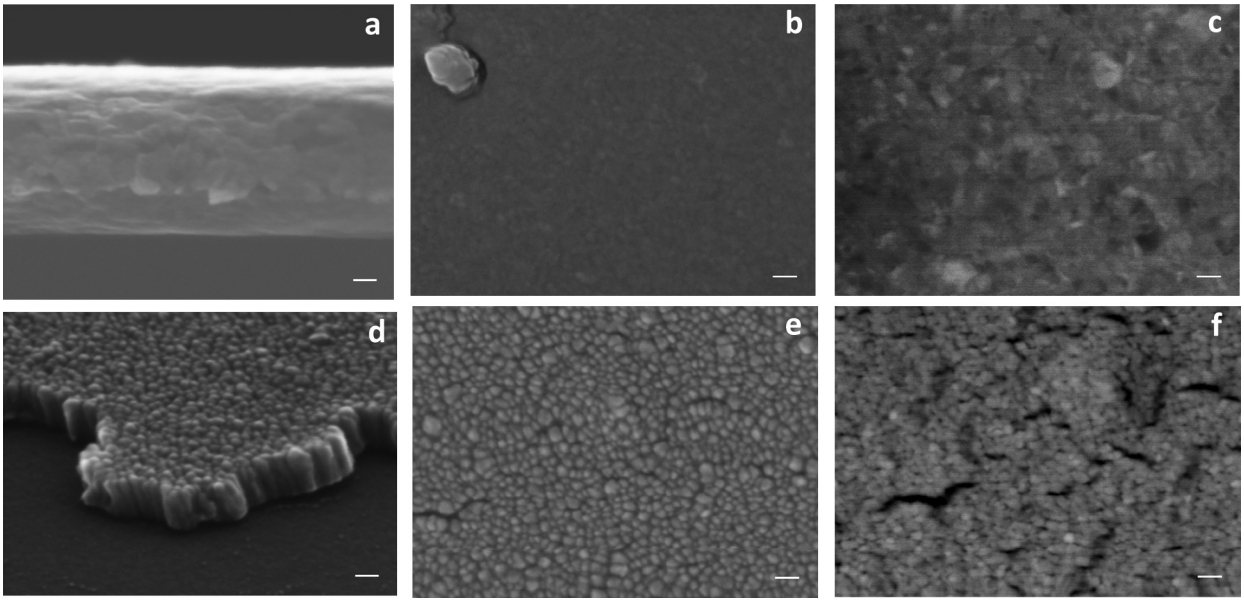

Fig. 1 – a, d) cross sectional and c, e) top view of dense and nano-columnar, respectively, Pd films grown on Si substrate; c) and f) grain contrast images of dense and nano-columnar Pd films. Size bar is 20 nm for all images.

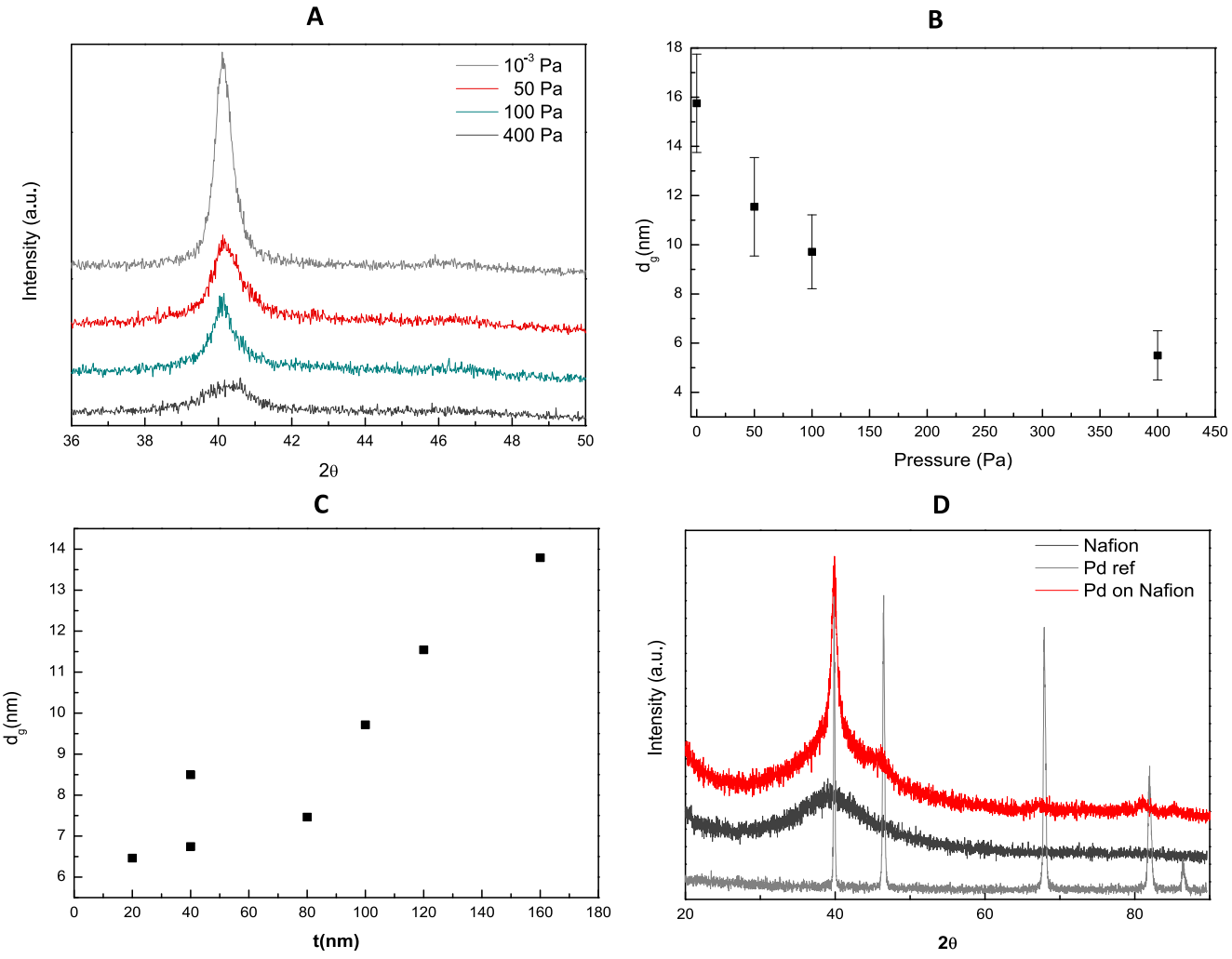

Fig. 2 – XRD analysis of nanostructured Pd films grown on Si and Nafion substrate: A) XRD for various He deposition pressures; grain size evolution with B) deposition pressure (sample thickness 100 nm) and C) thickness (deposition pressure 50 Pa); D) XRD of 50 Pa Pd film deposited on Nafion117™ with references (pristine Nafion117™ and Pd).

is increased by ca. 10 °C in comparison with the reference Nafion117™[1] (no barrier). On the other hand, the maximum of tan δ decreases from ca. 0.5 (no barrier) to ca. 0.4 (all the barriers), as shown in Fig. 4. This latter evidence is an indication that in all the barriers a smaller fraction of the overall mechanical energy provided to the system is dispersed by the α_{PC} relaxation mode [27]. Thus, it can be hypothesized that in all the barriers the hydrophobic fluorocarbon domains of Nafion are larger in comparison with the reference Nafion117™ (no barrier). This interpretation is also consistent with the lower storage modulus of the barriers in comparison with the reference Nafion117™ (no barrier).

The $\sigma'(\omega)$ spectra of the reference Nafion117™ (no barrier) and of the 200 nm/50 Pa barrier are reported in Fig. 5 and Fig. 6, respectively. The corresponding spectra of the 200 nm/1 Pa and the 50 nm/50 Pa barriers are shown in Supplementary Data. As a general trend, it is observed that the BES spectrum of the pristine reference Nafion117™ (see the upper panel of Fig. 5) is significantly simpler in comparison with those of all the pristine barriers (see the upper panel of Fig. 6 and Supplementary Data). In the latter spectra, at least two plateaus are always clearly evident. In particular: (a) a first plateau emerges progressively from the lowest frequencies and shifts up to ca. 10^4 Hz as T is raised up to 155 °C; and (b) a second plateau is observed at high frequencies (f higher than ca. 10^6 Hz) even at the lowest T; as the temperature is raised, this second plateau becomes somewhat masked by stray inductance effects originated by the cell setup [28]. These features are interpreted admitting that the pristine barriers are characterized by a complex microstructure showing a clear phase separation between large hydrophobic fluorocarbon domains and relatively small polar domains [29]. The phase separation gives rise to polarization effects which are at the basis of the formation of the observed two plateaus in the

[1] The DuPont Oval Logo, DuPont™, The miracles of science™ and all products denoted with a ™ and ® are trademarks or registered trademarks of DuPont or its affiliates."

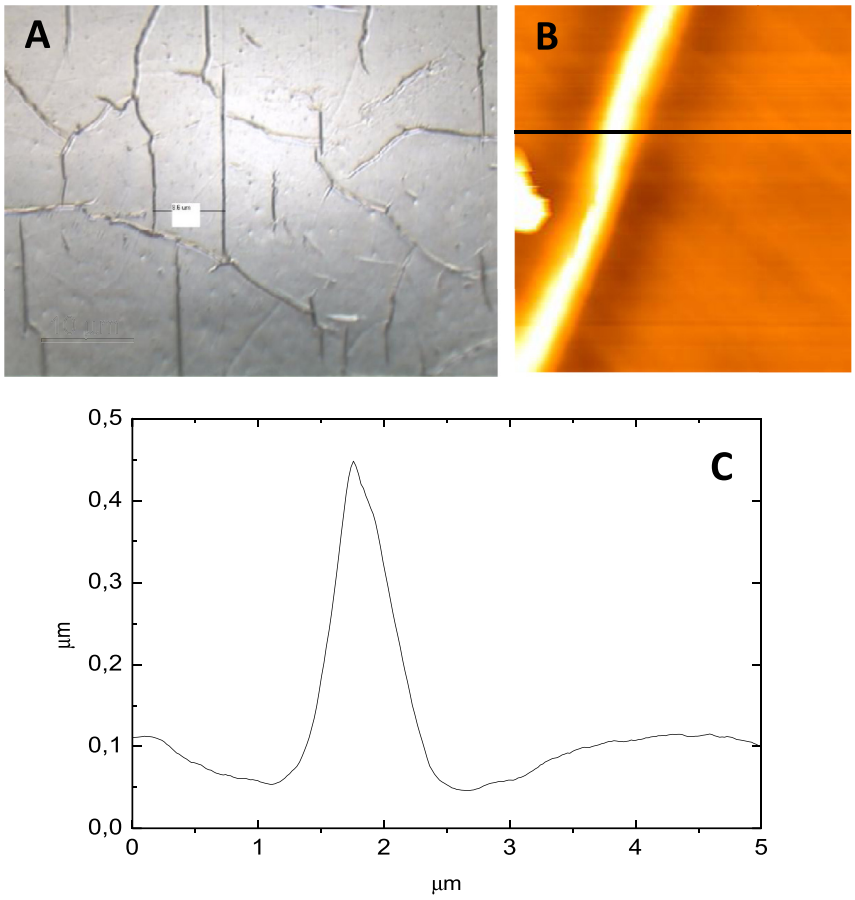

Fig. 3 – A) Pd deposited membrane after a week of storage in air; B) AFM of 5 × 5 μm area and C) corresponding line scan showing the topography of a buckled area.

$\sigma'(\omega)$ spectra [29]. The BES spectrum of the pristine reference Nafion117™ does not show clearly the first plateau since its hydrophobic fluorocarbon domains are most likely very small, yielding a less clear phase separation in comparison with the pristine barriers. The thermal history of a ionomeric material is known to affect significantly its charge transport properties [30]. For this reason, it is customary to apply a hydrothermal treatment to the samples, with the aim to achieve the same starting reference condition [18,30]. The reference Nafion117™ and all the barriers have undergone such a treatment (see the Experimental section), giving rise to the "hydrated" samples; the corresponding BES spectra are shown in the upper panels of Figs. 5 and 6 and in Supplementary data. The comparison between the BES spectrum of each pristine sample with the corresponding hydrated sample highlights that: (a) only one high-frequency plateau is observed; (b) the values of $\sigma'(\omega)$ are higher in the hydrated samples; and (c) the effect of the temperature on the $\sigma'(\omega)$ spectra in the hydrated samples is lower. These evidences are interpreted admitting that the hydrothermal treatment adopted to prepare the hydrated samples: (a) reduces the size of the hydrophobic fluorocarbon domains; (b) facilitates the contact between the polar domains, which become swollen with water. The values of the bulk conductivity σ_{DC} of the pristine and the hydrated samples are reported in the upper and lower panel of Fig. 7, respectively. It is highlighted that the pristine samples show σ_{DC} values in the order of ca. $10^{-4} - 10^{-2}$ S cm^{-1}; σ_{DC} increases by ca. 1.5 orders of magnitude as the temperature is raised up to 155 °C. This behaviour is typical of ion-conducting systems where the charge transport mechanism is a thermally-activated process [31]. On the other hand, in the hydrated samples: (a) σ_{DC} is higher in comparison with the pristine samples; (b) all the samples have very similar σ_{DC} for T lower than ca. 100 °C; (c) σ_{DC} of the barriers increases as T is raised up to 155 °C; and (d) σ_{DC} of reference Nafion117™ drops sharply at T higher than 100 °C. These evidences are coherent with the proposed evolution of the microstructure of the samples upon applying the hydrothermal process. In the hydrated samples, the swollen polar domains come into contact more easily following the relaxations of the hydrophobic fluorocarbon domains. Thus, the long-range charge transport is facilitated and σ_{DC} is increased in comparison with the pristine samples. It is highlighted that after the hydrothermal process the microstructures of the reference Nafion117™ and of all the barriers are expected to become quite similar, as witnessed by the disappearance of the first plateau at low frequencies in the $\sigma'(\omega)$ spectra and by the very similar σ_{DC} values shown by all the samples at T lower than ca. 100 °C. The barriers improve

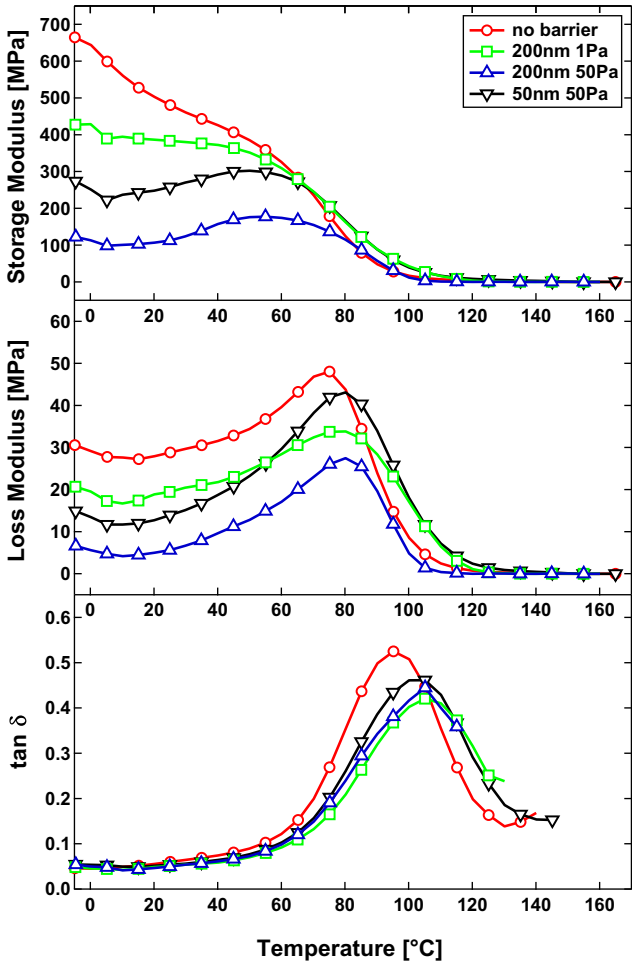

Fig. 4 – Temperature spectra of storage modulus (E′, upper panel), loss modulus (E″, middle panel) and tan δ vs. temperature for the membranes.

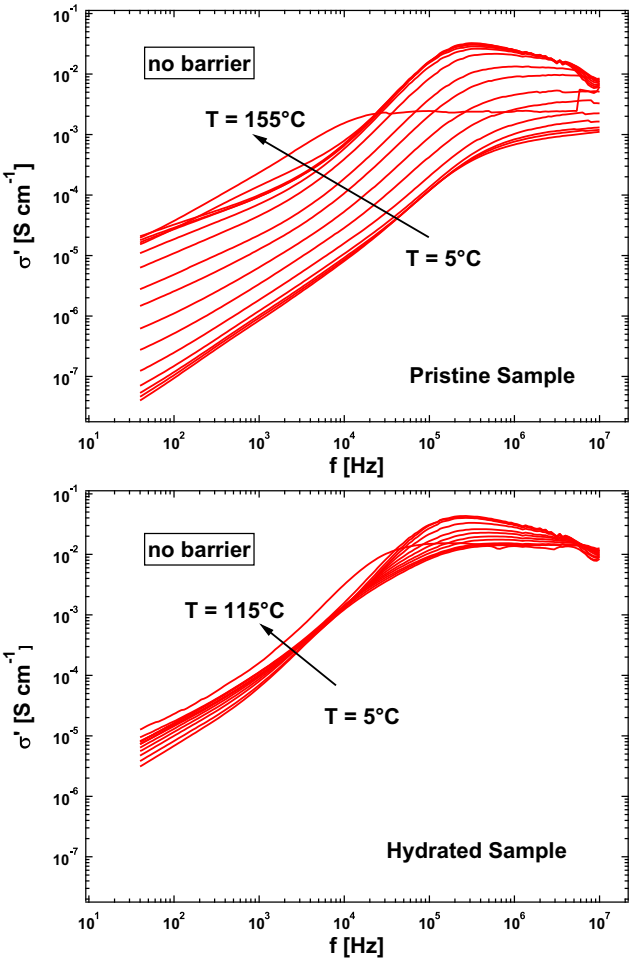

Fig. 5 – Real conductivity spectra of reference Nafion117™ (no barrier) between 5 and 155 °C. Pristine sample (upper panel); hydrated sample (lower panel).

the thermal stability of the hydrated samples, extending the stability range of conductivity (SRC) up to the highest investigated temperatures. The SRC is the temperature interval where the conductivity of a ionomeric membrane increases as *T* is raised [18,31]. In the absence of the barriers, the SRC of the reference Nafion117 extends up to only ca. 100 °C, consistently with results reported elsewhere [32].

3.3. *Fuel cell characterization*

In Figs. 8 and 9 methanol crossover measurements are reported for different Pd barriers and in different operating conditions. A considerable crossover reduction is evident in all the investigated cases. In particular a reduction included between 53% and 58% at open circuit voltage (OCV) is observed with the 200 nm/50 Pa barrier, compared to the MEA without barrier, irrespectively to the investigated operating conditions: variations in temperature and methanol concentration do not vary significantly such reduction, confirming barrier stability and results reliability. Note that the presence of a Pd barrier is still advantageous during operation at high methanol concentration and high current density, Fig. 9. The achieved effectiveness of the barrier is not consistent with the barrier and membrane characteristic reported in the previous sections, higher values are expected, considering film compactness. Analysing the samples after fuel cell testing the origin of such values is clarified: cracks are formed probably during fuel cell assembling process, Fig. 10, hindering the barrier effectiveness.

The MEA with 200 nm/1 Pa barrier presents a lower crossover reduction, about 30–38% at OCV: probably the deposition of a more dense film induces a more diffuse cracks formation, therefore, even at constant film thickness, the membrane area effectively covered by the film is lower than the case with the more porous 200 nm/50 Pa barrier. Reducing the Pd film to 50 nm the behaviour is consistent with the smaller grain size, more grain boundary and more chance for permeation: crossover reduction effectiveness is approximately halved, 18–23%. So a non-linear dependence on thickness is observed, the origin could be also related to less crack formation during assembling, thanks to improved mechanical characteristics.

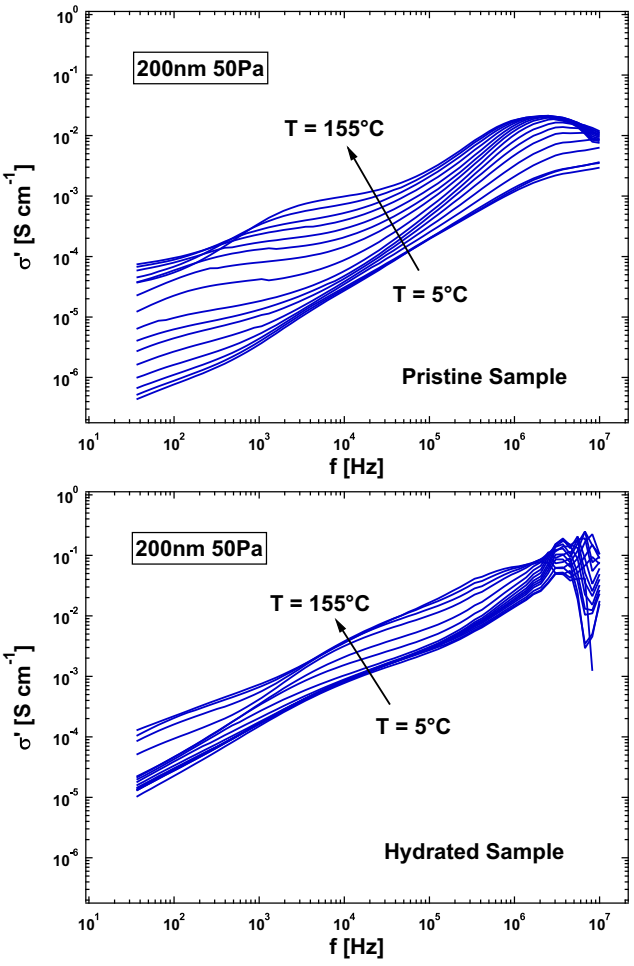

Fig. 6 – Real conductivity spectra of 200 nm/50 Pa barrier between 5 and 155 °C. Pristine sample (upper panel); hydrated sample (lower panel).

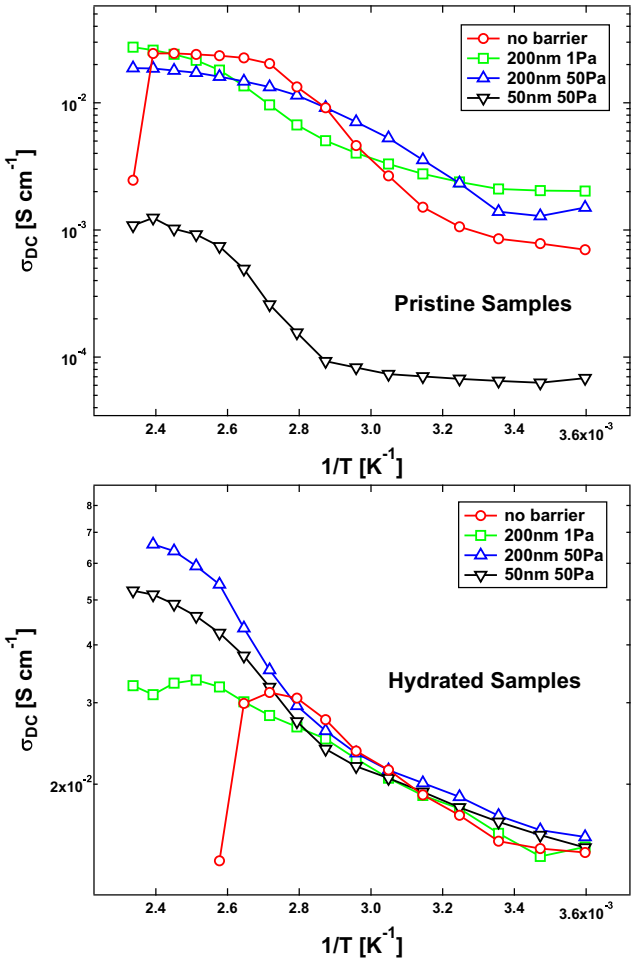

Fig. 7 – Bulk conductivity of the barriers as a function of the temperature. Pristine samples (upper panel); hydrated samples (lower panel).

In Fig. 11 the performance of MEA's with different barrier are reported: introducing the barrier higher voltages are observed at low current density in all the investigated conditions. As expected, reducing methanol crossover permits to decrease cathode overpotential related to mixed potential formation [12].

The MEA's with 200 nm/1 Pa and 50 nm/50 Pa barriers present very similar behaviours, consistently with similar density and grain size: a higher voltage than the reference case just till 0.2 A cm^{-2} and a stiff slope at high current density. The origin can be associated mainly to a lower membrane proton conductivity. In Fig. 12 membrane AC resistance measures at 1 kHz are reported: the Pd barriers effectively determine an increase of membrane resistance, that can explain the performance worsening and is quantitatively consistent with its magnitude. In the case with 200 nm/50 Pa barrier the performance reduction is even worse, the voltage is higher than the reference case just till 0.07 A/cm^2; coherently the membrane resistance is considerably higher, approximately the double of reference case at OCV.

Membrane resistance diminishes increasing the current density, thanks to a better membrane hydration operated by an enhanced water transport, i.e. more intense water production in the cathode electrode and electrosmotic drag [33]. Such behaviour is strongly incremented by the presence of the Pd barrier that hinders the water transport. As a consequence, the membrane resistance at low current density is strongly increased by a worse membrane hydration. Analysing the different barriers, a correlation between membrane resistance increase and methanol crossover reduction is evident: the more effective is the barrier to reduce methanol crossover and consequently water transport, the worse are membrane hydration and conductivity.

However the proton resistance of Pd barriers is not very significant, in fact at high current density, where membrane hydration is enhanced, the membrane resistance values are comparable with reference case.

The structural changes originated in the membranes during the deposition of the Pd barriers are not expected to affect significantly DMFC performance. Indeed, in the proposed operating conditions (i.e., feeding with 1–2 M methanol

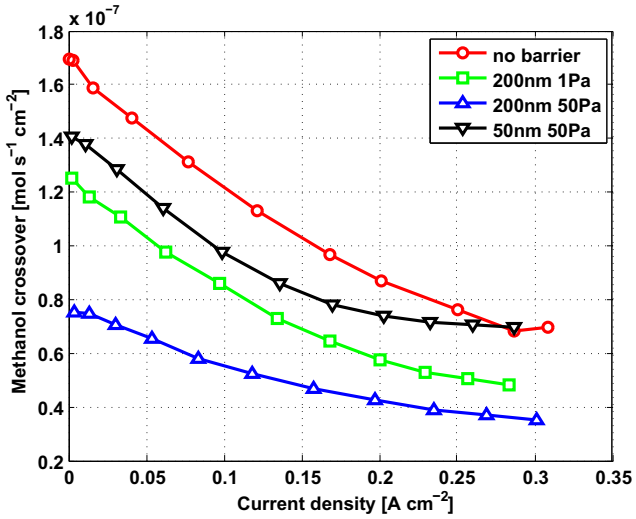

Fig. 8 – Methanol crossover varying current density for MEA's with different barriers (methanol concentration 1 M, temperature 60 °C).

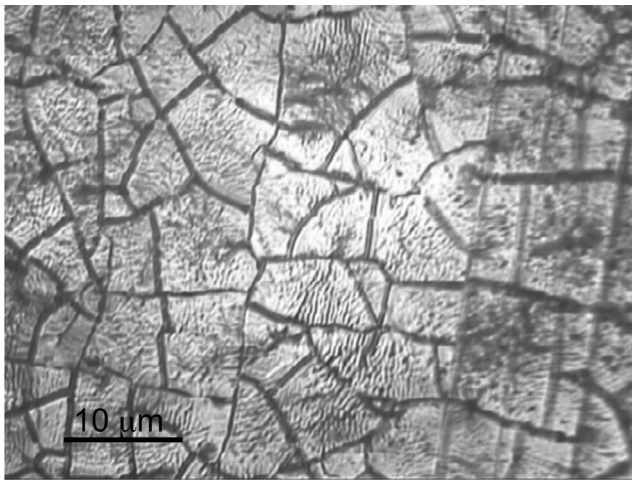

Fig. 10 – Pd deposited membrane after fuel cell testing.

solutions in water, $T = 60\ ^{\circ}C$) it is expected that the hydrophilic domains of all the membranes are swollen with water. Thus, a situation very similar in comparison with the membranes studied "ex situ" after the hydrothermal treatment is achieved, where all the systems share a similar through-plane conductivity (see Fig. 7). Thus, DMFC performance is mainly affected by the Pd barriers and their effects on other membrane properties (e.g. methanol crossover).

Analysing the efficiency of the different MEA's in function of power density, calculated as in Refs. [12], we can state that the Pd barriers permit to enhance considerably the efficiencies, in all the investigated conditions Fig. 13. Note that the operating conditions should be optimized for each material to maximize performance as a trade-off between efficiency and power density, considering application requirements; in the following analysis the comparison is carried out at fixed conditions.

The MEA with 200 nm/50 Pa barrier presents a maximum efficiency of 25%, compared to 20,5% of the reference case; a still higher increment is achieved at lower power density. To such efficiency increment is associated a reduction of maximum power density in the investigated conditions. Increased efficiencies, 22,4% and 21,6%, at similar power density are instead achievable introducing the 200 nm/1 Pa and 50 nm/50 Pa barriers. Therefore the characteristics of the barrier should be optimized considering application and cost requirements.

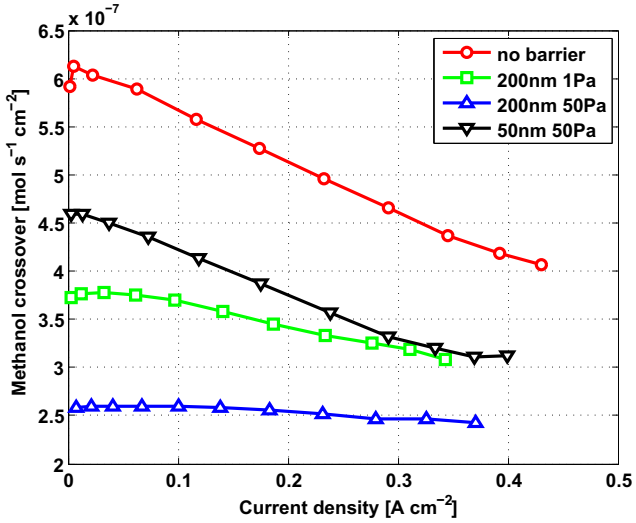

Fig. 9 – Methanol crossover varying current density for MEA's with different barriers (methanol concentration 2 M, temperature 80 °C).

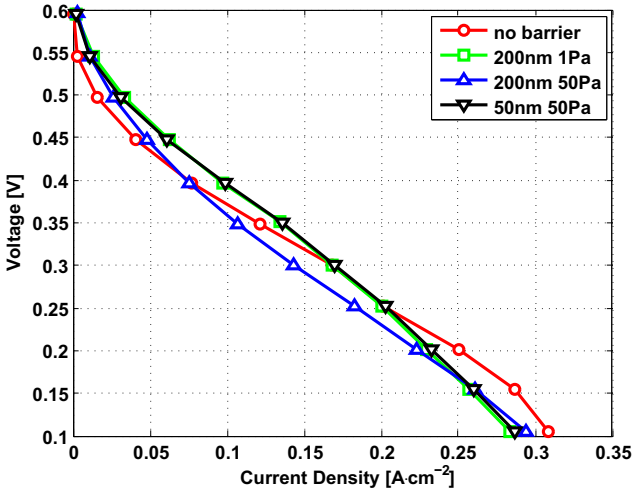

Fig. 11 – Polarization curves of MEA's with different barriers (methanol concentration 1 M, temperature 60 °C).

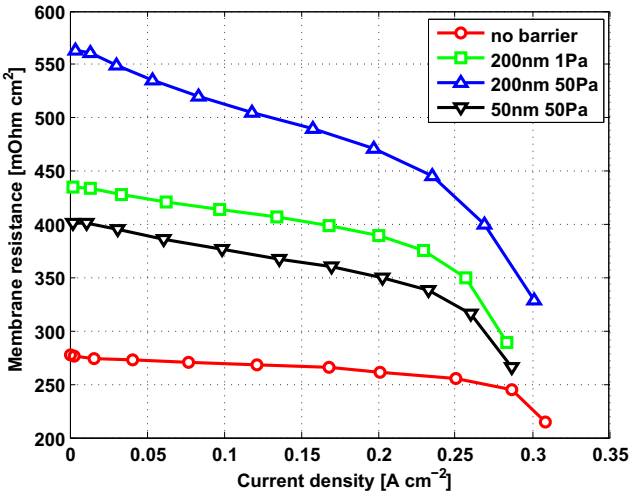

Fig. 12 – AC membrane resistance at 1 kHz varying current density for MEA's with different barriers (methanol concentration 1 M, temperature 60 °C).

4. Conclusion

This work demonstrated that Pulsed Laser Deposition technique is able to produce Pd barriers with controlled characteristics on standard perfluorosulfonic acid membranes even at pressures of several Pascals, able to reduce considerably methanol crossover in direct methanol fuel cell.

The DMA and BES investigations highlight that the deposition of the barriers alters the microstructure of the Nafion117™ membranes used as the substrate. In particular, it is expected that additional crosslinks are formed in the polar domains of Nafion, while the size of the hydrophobic fluorocarbon domains is increased. However, these alterations in the microstructure of the Nafion ionomer are cancelled by the hydrothermal treatment adopted to obtain the hydrated samples, or by the conditioning process used before the fuel cell tests. As a result, all the membranes mounted in the DMFCs probably share the same microstructure; thus, the conductivity is only affected by the amount of water present in each membrane. The conductivity of the membranes is increased as the amount of water is raised; this interpretation is consistent both with the fuel cell tests and with the BES results reported elsewhere [28].

The Pd barriers permit to reduce methanol crossover by more than 50%, increasing significantly the fuel cell efficiency, admitting a slight power density reduction. At similar power density, a methanol crossover reduction of 30% can be achieved, improving consequently fuel cell efficiency. Barriers produced at higher pressure are more effective in reducing crossover, due to a more nanocolumnar and porous structure that limits cracks formation. This phenomenon is suspected to be also the origin of the observed non-linear dependence of membrane effectiveness on thickness. However the developed Pd barriers hindered methanol transport through the membrane as well as water transport, worsening membrane hydration at low current density. Therefore the characteristics of the Pd barrier should be optimized together with operating conditions, to maximize performance, satisfying application requirements.

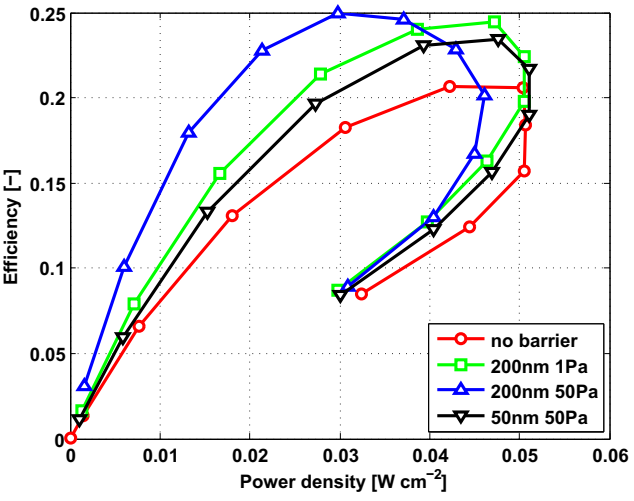

Fig. 13 – Fuel cell efficiency varying power density for MEA's with different barriers (methanol concentration 1 M, temperature 60 °C).

Acknowledgement

Funding for this work from Fondazione Cariplo under agreement no. 2007.5543 is acknowledged. F. Di Fonzo thanks Claudia Conti for XRD measurements and M. Fusi for AFM images. E. Negro thanks Regione del Veneto (SMUPR n. 4148, Polo di ricerca del settore fotovoltaico) for financial support.

Appendix A. Supplementary data

Supplementary data related to this article can be found on line.

REFERENCES

[1] Di Noto V, Zawodzinski TA, Herring AM, Giffin GA, Negro E, Lavina S. Polymer electrolytes for a hydrogen economy. International Journal of Hydrogen Energy 2012;37:6120–31.

[2] Heinzel A, Barragan VM. A review of the state-of-the-art of the methanol crossover in direct methanol fuel cells. Journal of Power Sources 1999;84:70–4.

[3] Dohle H, Divisek J, Mergel J, Oetjen HF, Zingler C, Stolten D. Recent developments of the measurement of the methanol permeation in a direct methanol fuel cell. Journal of Power Sources 2002;105(2):274–82.

[4] Qi Z, Kaufman A. Open circuit voltage and methanol crossover in DMFCs. Journal of Power Sources 2002;110(1):177–85.

[5] Gogel V, Frey T, Yongsheng Zhu, Friedrich KA, Jorissen L, Garche J. Performance and methanol permeation of direct methanol fuel cells: dependence on operating conditions and on electrode structure. Journal of Power Sources 2004;127(1–2):172–80.

[6] Casalegno A, Grassini P, Marchesi R. Experimental analysis of methanol cross-over in a direct methanol fuel cell. Applied Thermal Engineering March 2007;27.
[7] Antonucci PL, Arico AS, Creti P, Ramunni E, Antonucci V. Investigation of a direct methanol fuel cell based on a composite Nafion-silica electrolyte for high temperature operation. Solid State Ionics 1999;125(1–4):431.
[8] Yang C, Srinivasan S, Arico AS, Creti P, Baglio V, Antonucci V. Composition Nafion/zirconium phosphate membranes for direct methanol fuel cell operation at high temperature. Electrochemical Solid State Letters 2001;4(4):A31.
[9] Uchida H, Mizuno Y, Watanabe M. Suppression of methanol crossover in Pt-dispersed polymer electrolyte membrane for direct methanol fuel cells. Chemistry Letters 2000;(11):1268.
[10] Jia N, Lefebvre MC, Halfyard J, Qi Z, Pickup PG. Modification of Nafion proton exchange membranes to reduce methanol crossover in PEM fuel cells. Electrochemical Solid State Letters 2000;3(12):529.
[11] Peled E, Duvdevani T, Aharon A, Melman A. A direct methanol fuel cell based on a novel low-cost nanoporous proton-conducting membrane. Electrochemical Solid State Letters 2000;3(12):525.
[12] Casalegno A, Santoro C, Rinaldi F, Marchesi R. Low methanol crossover and high efficiency direct methanol fuel cell: the influence of diffusion layers. Journal of Power Sources 2011;196:2669–75.
[13] Lewis FA. The palladium-hydrogen system. Platinum Metals Review 1982;26(2):70.
[14] Ma ZQ, Cheng P, Zhao TS. A palladium-alloy deposited Nafion membrane for direct methanol fuel cells. Journal of Membrane Science 2003;215:327–36.
[15] Prabhuram J, Zhao TS, Liang ZX, Yang H, Wong CW. Pd and Pd–Cu alloy deposited nafion membranes for reduction of methanol crossover in direct methanol fuel cells. Journal of The Electrochemical Society 2005;152(7):A1390–7.
[16] Knapton AG. Palladium alloys for hydrogen diffusion membranes. Platinum Metals Review 1977;21(2):44.
[17] Di Noto V, Boaretto N, Negro E, Pace G. New inorganic–organic proton conducting membranes based on Nafion and hydrophobic fluoroalkylated silica nanoparticles. Journal of Power Sources 2010;195:7734–42.
[18] Di Noto V, Piga M, Lavina S, Negro E, Yoshida K, Ito R, et al. Structure, properties and proton conductivity of Nafion/$[(TiO_2)\cdot(WO_3)_{0.148}]\psi TiO_2$ nanocomposite membranes. Electrochimica Acta 2010;55:1431–44.
[19] Movchan BA, Demchishin AV. Investigation of the structure and properties of thick vacuum-deposited films of nickel, titanium, tungsten, alumina and zirconium dioxide. Fizika Metallov i Metallovedenie (Physics of Metals and Metallography) 1969;28:653.
[20] Thornton JA. Influence of apparatus geometry and deposition conditions on the structure and topography of thick sputtered coatings. Journal of Vacuum Science & Technology 1974;11:666.
[21] Infortuna A, Harvey A, Gauckler LJ. Microstructures of CGO and YSZ thin films by pulsed laser deposition. Advanced Functional Materials 2008;18:127–35.
[22] Vasco E, Polop C, Sacedon. Preventing kinetic roughening in physical vapor-phase-deposition films, JL. Physical Review Letters 2008;100:016102.
[23] García Ferré F, Bertarelli E, Chiodoni A, Carnelli D, Gastaldi D, Vena P, et al. The mechanical properties of a nanocrystalline Al2O3/a-Al2O3 composite coating measured by nanoindentation and brillouin spectroscopy. Acta Materialia 2013;61(7):2662–70.
[24] Di Fonzo F, Tonini D, Li Bassi A, Casari C, Beghi M, Bottani C, et al. Growth regimes in pulsed laser deposition of aluminum oxide films. Applied Physics A: Materials Science & Processing 2008;93:765–9.
[25] Fonzo FD, Casari CS, Russo V, Brunella MF, Li Bassi A, Bottani CE. Hierarchically organized nanostructured TiO2 for photocatalysis applications. Nanotechnology 2009;20:015604.
[26] Canovic S, Jonsson T, Halvarsson M. "Grain contrast imaging in FIB and SEM. Journal of Physics: Conference Series 2008;126(012054):1–4.
[27] Di Noto V, Bettiol M, Bassetto F, Boaretto N, Negro E, Lavina S, et al. Hybrid inorganic-organic nanocomposite polymer electrolytes based on Nafion and fluorinated TiO_2 for PEMFCs. International Journal of Hydrogen Energy 2012;37:6169–81.
[28] Di Noto V, Fontanella JJ, Wintersgill MC, Giffin GA, Vezzù K, Piga M, et al. Pressure, temperature and dew point broadband electrical spectroscopy (PTD-BES) for the investigation of membranes for PEMFCs. Fuel Cells 2013;13:48–57.
[29] Di Noto V, Piga M, Giffin GA, Lavina S, Smotkin ES, Sanchez JY, et al. Influence of anions on proton-conducting membranes based on neutralized nafion 117, triethylammonium methanesulfonate, and triethylammonium perfluorobutanesulfonate. 2. Electrical properties. Journal of Physical Chemistry C 2012;116:1370–9.
[30] Alberti G, Narducci R, Sganappa M. Effects of hydrothermal/thermal treatments on the water-uptake of Nafion membranes and relations with changes of conformation, counter-elastic force and tensile modulus of the matrix. Journal of Power Sources 2008;178:575–83.
[31] Di Noto V, Negro E, Lavina S, Vittadello M. Hybrid inorganic-organic polymer electrolytes. In: Sequeira C, Santos D, editors. Polymer electrolytes – fundamentals and applications, 6. Oxford: Woodhead Publishing Limited; 2010. p. 219–77.
[32] Di Noto V, Lavina S, Negro E, Vittadello M, Conti F, Piga M, et al. Hybrid inorganic-organic proton conducting membranes based on Nafion and 5 wt% of M_xO_y (M = Ti, Zr, Hf, Ta and W). Part II: relaxation phenomena and conductivity mechanism. Journal of Power Sources 2009;187:57–66.
[33] Zago M, Casalegno A, Santoro C, Marchesi R. Water transport and flooding in DMFC: experimental and modeling analyses. Journal of Power Sources 2012;217:381–91.